
Proceedings Paper:
Liu, J., Sugiyama, H., Nakayama, T. et al. (1 more author) (2020) Magnetic sensor based topographic localization for automatic dislocation of ingested button battery. In: 2020 IEEE International Conference on Robotics and Automation (ICRA). ICRA 2020, 31 May - 31 Aug 2020, Virtual conference. IEEE . ISBN 9781728173962

https://doi.org/10.1109/ICRA40945.2020.9196546

Magnetic Sensor Based Topographic Localization for Automatic Dislocation of Ingested Button Battery

Jialun Liu[1*], Hironari Sugiyama[2,1], Tadachika Nakayama[2], and Shuhei Miyashita[1]

***Abstract*— A button battery accidentally ingested by a toddler or small child can cause severe damage to the stomach within a short period of time. Once a battery lands on the surface of the esophagus or stomach, it can run a current in the tissue and induce a chemical reaction resulting in injury. Following our previous work where we presented an ingestible magnetic robot for button battery retrieval, this study presents a remotely achieved novel localization method of a button battery with commonly available magnetic sensors (Hall-effect sensors). By applying a direct magnetic field to the button battery using an electromagnetic coil, the battery is magnetized, and hence it becomes able to be sensed by Hall-effect sensors. Using a trilateration method, we were able to detect the locations of an LR44 button battery and other ferromagnetic materials at variable distances. Additional four electromagnetic coils were used to autonomously navigate a magnet-containing capsule to dislocate the battery from the affected site.**

I. Introduction

Accidental ingestion of a button battery is a frequently reported incidence, happening to over 3000 people every year in the US alone [1]. Most of the victims are toddlers and children, between 0 and 6 years of age, accounting for 87% of these incidences. Several studies have shown that the lining of the stomach can be burnt in just two hours after ingestion [2] and ulcerations can occur in five hours [3], whereas the conventional endoscopic examination requires a difficult surgical operation by an expert.

The magnetically actuated microrobots *in vivo* operations have been shown to have the potential to positively impact current medical treatments by, for example, allowing surgeries to be conducted in a minimally invasive way [4]–[10].

With an embedded camera and wireless actuation technique, untethered robotic capsule endoscopes show a new approach for performing diagnostic and therapeutic medical operations for the gastrointestinal disease [11]–[18]. This technique is not restricted to use in the GI tract; several studies have shown its usefulness in ophthalmologic procedures [19], remote manipulation of magnetic bacteria [20], tissue regeneration [21], and intravascular therapy [22].

In our previous work, we presented an ingestible origami patch that can be instantly deployed inside the stomach and visually guided to dislocate a harming button battery at a wound site [23]–[25]. As alternatives to visual tracking for the localization of magnetic robots, magnetic sensors provide a low-cost and efficient solution [9], [26]–[30].

[1]Department of Automatic Control and System Engineering, University of Sheffield, Sheffield S1 3JD, UK. shuhei.miyashita@sheffield.ac.uk [2]Department of Science of Technology Innovation, Nagaoka University of Technology, 1603-1 Kamitomioka, Nagaoka, Niigata, Japan. *Corresponding author.

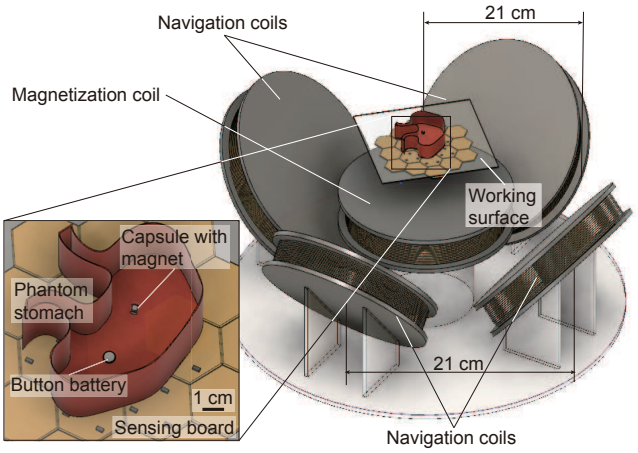

Fig. 1. The proposed system. The horizontal magnetization coil is used to magnetize the button battery. The magnetized battery is then sensed by Hall-effect sensors. Four surrounding coils are used to navigate an interventional magnetic capsule for dislocation purpose.

The detection and localization of an ingested battery, on the other hand, is still a problem needing an accessible technique that does not depend on costly medical imaging modalities such as ultrasound, fluoroscopic imaging or MRI. The plain radiograph or nuclear medicine (PET) appears to be superior as its accuracy however it is invasive by radiation. The classical metal detection method of detecting magnetic resonance, however, is not a viable alternative as it requires a probe with a diameter larger than the targeted ferromagnetic object and it requires the active repositioning of that probe [31]–[33].

As a solution to this problem, this study proposes a novel method for the localization of a button battery. Noting that a ferromagnetic material, including a button battery, can be remotely magnetized by the application of an electromagnetic field, we demonstrate that it is possible to actively sense the location of the battery by simply combining an electromagnetic coil with spatially distributed Hall-effect sensors. The contributions of the paper are:

1) to present the concept of the active sensing of a button battery by remotely magnetizing it and detecting its presence and location with magnetic sensors.
2) to model the localization of a button battery and the experimental verification.
3) to demonstrate the autonomous dislocation of a button battery in a phantom stomach using an interventional magnetic capsule.

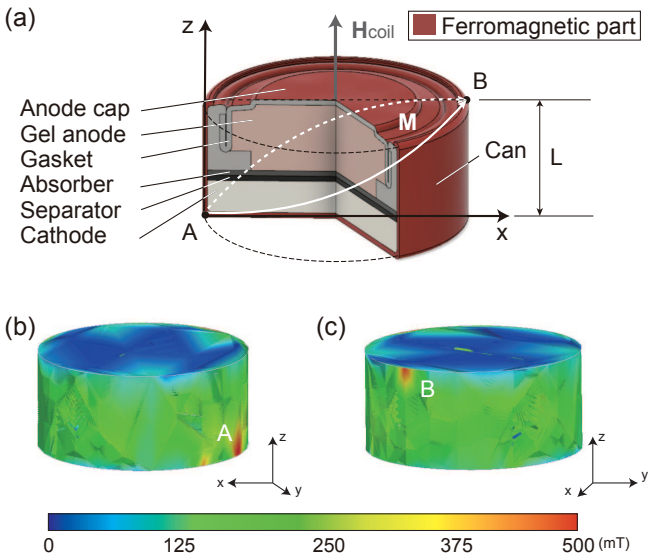

Fig. 2. LR44 button battery and its composition. (a) The dissection of LR44 battery. (b)(c) Finite element analysis of magnetic flux density when a magnetic field is applied along the positive direction of z-axis to a horizontal sitting battery.

II. Methods

This method of detecting the location of a button battery is based on the assumption that a button battery can be remotely magnetized with a direct magnetic field to a magnetic strength level such that it can be sensed by Hall-effect sensors. In this section, we will model the magnetization of a button battery under a magnetic field, followed by the method of trilateration using Hall-effect sensors. To begin, we use the LR44 alkaline button battery, which is the most commonly used button battery. Different types of button battery are investigated and discussed in Section IV. We consider two postures: "horizontal sitting" where a battery sits horizontally, placing the circular top or bottom face on the ground, and "overturned sitting" where the battery position places its cylindrical face on the ground.

A. Remote magnetization of button battery

Fig. 2 (a) shows the dissection of an LR44 button battery. The battery consists of multiple materials; the ferromagnetic part (made of ferritic stainless steel) that reacts to magnetic input is located at the exterior of the body, called anode cap and can and colored red. Thus, a button battery can be modeled as a hollow ferromagnetic cylindrical object with outer radius of $5.75\,\text{mm}$, inner radius of $5.25\,\text{mm}$, and height L ($= 5.4\,\text{mm}$), and having a top and a bottom surface with the same thickness of $0.5\,\text{mm}$. Generally speaking, stainless steel is resistant to alkali; therefore, the chemical reactions of the ingested button battery inside the stomach (mainly the generation of an external electrolytic current that hydrolyzes tissue fluids and produces hydroxide) would not affect the remote magnetization of the anode and the cathode. We estimated the principal magnetization $\mathbf{M}$ of a button battery under a magnetic field using the finite element method in ANSYS Maxwell. The results are shown in Fig. 2 (b)(c). In a ferromagnetic substance, magnetization under a magnetic field occurs along the longitudinal dimension of its body. Based on this fact, we assume that when an external magnetic field $\mathbf{H}_{coil}$ is applied to the button battery in the positive direction of z-axis, $\mathbf{M}$ is produced, as in Fig. 2 (a), which takes the shortest path connecting two farthest locations inside the ferromagnetic body, one corner (point A) and the other (point B), making them the South and North poles, respectively. In theory, due to the symmetry of the body and the magnetic field, A and B are not fixed at certain locations on the edges of the button battery.

In regards to the relatively low magnetic fields applied, the principal magnetization $\mathbf{M}$ of the ferromagnetic material is in the linear-magnetization region, thus $\mathbf{M}$ is approximately proportional to the applied magnetic field $\mathbf{H}_{coil}$.

In the case of a horizontal sitting battery, $\mathbf{H}_{coil}$ is perpendicularly applied to the button battery, poles A and B change arbitrarily on the edges. However, the distance between two poles along z-axis remains unchanged ($=L$); therefore, the z component of the principal magnetic moment of the magnetized button battery m_z only relates to the intensity of the applied field,

$$m_z \propto \mathbf{H}_{coil}. \tag{1}$$

B. Localization

When a magnetized button battery is present, the Hall-effect sensor perceives a magnetic field both from the vertically applied field $\mathbf{H}_{coil}$ and the magnetized button battery,

$$\mathbf{B}_{sens} = \mathbf{B}_{coil} + \mathbf{B}_{mag}, \tag{2}$$

where $\mathbf{B}_{sens}$ is the magnetic flux density at the sensor, $\mathbf{B}_{coil}$ is the magnetic flux density of the vertical applied field $\mathbf{H}_{coil}$ at the sensor, produced by the magnetization coil in Fig. 1, and $\mathbf{B}_{mag}$ is the magnetic flux density of the magnetized button battery.

The magnetized button battery is modeled as a magnetic dipole with magnetic moment $\mathbf{m}$, thus the magnetic flux density in the space at distance $\mathbf{r}$ ($\mathbf{r} \gg 2c_1$) is

$$\mathbf{B}_{mag}(\mathbf{m}, \mathbf{r}) = \frac{\mu_0 \mathbf{m}}{4\pi}\left(\frac{3\mathbf{r}(\hat{\mathbf{m}}\cdot\mathbf{r})}{\|\mathbf{r}\|^5} - \frac{\hat{\mathbf{m}}}{\|\mathbf{r}\|^3}\right), \tag{3}$$

where μ_0 is the permeability of free space, $\mathbf{r}$ is a position vector pointing from the button battery position (x, y, z) to sensor position (x_s, y_s, z_s), and $\hat{\mathbf{m}}$ is the normalized vector in the direction of magnetic moment.

For the sake of simplicity, only the z component of $\mathbf{m}$, m_z is considered, i.e. $\hat{\mathbf{m}} = (0, 0, 1)$. The magnetic flux density in the z direction at the sensor, $\mathbf{B}^z_{mag}$ is therefore [28]

$$\begin{aligned}\mathbf{B}^z_{mag} &= \frac{\mu_0 \mathbf{m}}{4\pi}\left\{\frac{3}{\|\mathbf{r}\|^5}[\hat{m}_x(x_s - x) + \hat{m}_y(y_s - y) \right. \\ &\left. + \hat{m}_z(z_s - z)](z_s - z) - \frac{\hat{m}_z}{\|\mathbf{r}\|^3}\right\} \\ &= \frac{\mu_0 m_z}{4\pi}\left(\frac{3(z_s - z)^2}{\|\mathbf{r}\|^5} - \frac{1}{\|\mathbf{r}\|^3}\right),\end{aligned} \tag{4}$$

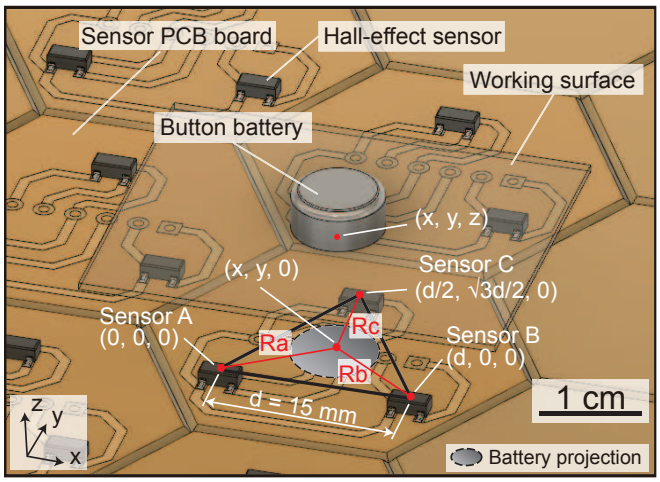

Fig. 3. Trilateration method using Hall-effect sensors. Each hexagonal sensor PCB board consists of three sensors. Every three nearby sensors form an equilateral triangle; therefore a triangular grid is created that allows to perform trilateration method in all triangles.

where $\|\mathbf{r}\|$ is the L_2 norm of the position vector, $\|\mathbf{r}\| = \sqrt{(x_s - x)^2 + (y_s - y)^2 + (z_s - z)^2}$.

The mono-axial Hall-effect sensors (Allegro A1389) used in the system are on a plane that is parallel to the working surface. Each sensor measures the magnetic field along the z-axis, therefore we only consider the magnetic flux density in z direction, thus (2) becomes $\mathbf{B}^z_{sens} = \mathbf{B}_{coil} + \mathbf{B}^z_{mag}$ where $\mathbf{B}^z_{sens}$ is the sensor measurement of $\mathbf{B}_{sens}$.

(1) indicates that when the applied magnetic field $\mathbf{B}_{coil}$ remains unchanged, m_z will also remain unchanged, hence $\mathbf{B}^z_{sens}$ only relates the distance from the battery to the sensor according to (4).

To determine the relation between the magnetic flux density at each sensor and the distance between the Hall-effect sensor and the button battery, we horizontally translated the magnetized button battery away from the sensor from 0 mm to 15 mm, and then took sensor measurements. A sigmoid function with four tunable parameters (p_1, p_2, p_3, p_4) is used to approximate the relation

$$\mathbf{B}^z_{sens} = f(R) = p_1 + \frac{(p_2 - p_1)}{1 + 10^{p_4(p_3 - R)}}, \tag{5}$$

where R is the distance between the sensor and the button battery. (p_1, p_2, p_3, p_4) were determined from the result in Section III-A. Once we know the magnetic flux density measured by the sensor, the distance R can be calculated by

$$R(\mathbf{B}^z_{sens}) = f^{-1}(\mathbf{B}^z_{sens}). \tag{6}$$

It is possible, therefore, to topographically estimate the position of the button battery using the trilateration method.

C. Trilateration

The basic method of trilateration is taken as demonstrated in [9], [28]. Fig. 3 shows the locations of the Hall-effect sensors and a button battery on the working surface. An array of Hall-effect sensors is arranged on multiple hexagonal PCB boards carpeting the space such that the covered area can be flexibly expanded. In each hexagonal board, three mono-axial Hall-effect sensors are implemented as an equilateral triangle with a side length of d (= 15) mm. We set the position of the bottom left sensor A in Fig. 3 to be $(0, 0, 0)$ in the global coordinate, sensor B $(d, 0, 0)$, and sensor C $(\frac{d}{2}, \frac{\sqrt{3}d}{2}, 0)$. The position of the button battery can hence be describable as (x, y, z) and its projection on the sensing board as $(x, y, 0)$. The distance between the plane of sensors and the button battery, z, is set as a variable.

After reading the magnetic flux density at sensor A, B and C along the z-axis, $\mathbf{B}^a_{sens}, \mathbf{B}^b_{sens}, \mathbf{B}^c_{sens}$, respectively, (6) converts the magnetic flux density to distance:

$$R_a = f^{-1}(\mathbf{B}^a_{sens}), \tag{7}$$
$$R_b = f^{-1}(\mathbf{B}^b_{sens}), \tag{8}$$
$$R_c = f^{-1}(\mathbf{B}^c_{sens}). \tag{9}$$

R_a, R_b, R_c indicate the radii of 3 spheres for trilateration method:

$$R_a^2 = x^2 + y^2 + z^2, \tag{10}$$
$$R_b^2 = (x - d)^2 + y^2 + z^2, \tag{11}$$
$$R_c^2 = \left(x - \frac{d}{2}\right)^2 + \left(y - \frac{\sqrt{3}d}{2}\right)^2 + z^2. \tag{12}$$

Combining (7), (8) and (9), (10), (11) and (12), the intersection of 3 spheres (x, y, z) is derived.

$$x = \frac{[f^{-1}(\mathbf{B}^a_{sens})]^2 - [f^{-1}(\mathbf{B}^b_{sens})]^2 + d^2}{2d}, \tag{13}$$
$$y = \frac{d^2 - xd - [f^{-1}(\mathbf{B}^c_{sens})]^2 + [f^{-1}(\mathbf{B}^a_{sens})]^2}{\sqrt{3}d}, \tag{14}$$
$$z = \pm\sqrt{[f^{-1}(\mathbf{B}^a_{sens})]^2 - y^2 - x^2}. \tag{15}$$

(15) indicates there are two candidates for z; since the button battery is above the sensor array, we keep z positive.

D. Hardware implementation and control algorithm

The electromagnetic coil system consists of four coils that are inclined 45° from the horizontal plane and placed at equal distances facing the approximate location of the button battery and one horizontal coil (Fig. 1). The four inclined coils (named navigation coils) are able to produce a superposed magnetic field in any direction at around the region where the axes of symmetry of the coils intersect and thus can be used to actuate a magnetic material on the working surface to drive the locomotion of a magnetically actuated robot [23], [25]. The horizontal coil (named magnetization coil) is newly created and placed in the middle of the inclined coils facing the targeted workspace and is used to produce a vertical magnetic field for remotely magnetizing the button battery. The working surface is 60 mm above the horizontal coil and the sensing board is 10 mm under the working surface. In our experiments, 7 hexagonal boards were implemented providing 25 available triangles for trilateration localization

TABLE I

SPECIFICATIONS OF EXPERIMENTAL SETUP

Item	Value
Electromagnetic system	
Navigation coils	4 counts, ∅ 21 cm
Magnetization coil	1 count, ∅ 20.4 cm
Electronic components	
Allegro A1389 Hall-effect sensors	21 counts
- Sensitivity	90 mV/mT
- Measurement range	± 27.8 mT
Sabertooth motor drivers	2 counts
- Usage	For navigation coils
- Maximum current	32 A
SyRen 25 motor driver	1 count
- Usage	For magnetization coil
- Maximum current	25 A
Capsule	$15 \times 8.4 \times 8.4\,\text{mm}^3$
- Permanent magnet in capsule	$5 \times 5 \times 5\,\text{mm}^3$
- Magnetic moment	$0.14\ \text{Am}^2$

method, offering $24.36\,\text{cm}^2$ sensing area. The specifications of the coils and the components used are listed in Table I.

In the automatic dislocation experiments, the control algorithm first actuates the magnetization coil to produce a vertical magnetic field, such that the location of the battery can be calculated through the sensory data based on the proposed trilateration localization method. Due to the weak magnetic field produced by the electromagnetic coil system, direct actuation of the magnetized button battery is impossible; therefore, a magnet-containing capsule is used to dislocate the capsule. Next, the system switches to the navigation mode, and the algorithm proceeds with the real-time tracking of the capsule and controls the navigation coils to navigate the capsule to the button battery and dislocate the battery. The pseudo code of the control algorithm is shown in **Algorithm 1**.

Algorithm 1 Main algorithm

```
function BATTERYDETECTION
    applyVerticalMagneticField()
    offset ← calibrateSensors()
    position ← trilaterialLocalization(offset)
    batteryPosition ← position
    return batteryPosition
end function
function TRILATERIALLOCALIZATION(offset)
    sensorData ← readSensors()
    sensorData ← sensorData − offset
    for each i ∈ numberOfSensors do
        activeSensors ← readSensorNode(i)
    end for
    activeTriangle ← getTriangle(activeSensors)
    position ← trilateration(activeTriangle)
    return position
end function
```

III. EXPERIMENTAL RESULTS

A. Sensitivity on different position of button battery

Fig. 4 shows the magnetic flux density at a sensor location ($\mathbf{B}^z_{sens}$) being measured by the Hall-effect sensor while $\mathbf{B}_{coil} = 8.23\,\text{mT}$ is applied, and relocating the position of the LR44 button battery along the x-axis (0 mm to 15 mm, which is the distance between the normal axes) and the z-axis (8 mm to 15 mm, which is the distance between the closest surfaces). The LR44 button battery has a diameter of 11.5 mm and a height of 5.4 mm. In theory, a non-zero gradient in the plot assures that detection is possible for the transition despite the sensitivity of the signal. In practice, a smaller gradient indicates less difference in the sensor readings while the button battery is moving away from the sensor, which gives a weaker performance in button battery detection. Also, we tested the maximum sensible range of the button battery was 31.6 mm while $\mathbf{B}_{coil} = 8.23\,\text{mT}$ is applied. For a discussion on improving the sensing range, see Section IV-A.

B. Magnetization of button battery

Experiment was conducted to see the magnetization effect of an LR44 button battery. A horizontal sitting battery was placed on the working surface with an applied field of 8.54 mT on the sensing board. We measure the magnetic flux density on the sensing board using a Gauss meter; the results are shown in Fig. 5. The heat map demonstrates a clear magnetic flux density difference on the sensing board when the button battery is present, proving the feasibility of our method.

Additional experiment investigated the magnetization of the button battery when different vertical fields $\mathbf{B}_{coil}$ are applied. An LR44 battery was placed 10 mm above where a Hall-effect sensor is located ($z = 0.01$). We increased the magnetic flux density of the applied field $\mathbf{B}_{coil}$ from 0 mT to 11.1 mT and recorded the magnetic flux density measured by the Hall-effect sensor. Fig. 6 (a) shows the difference

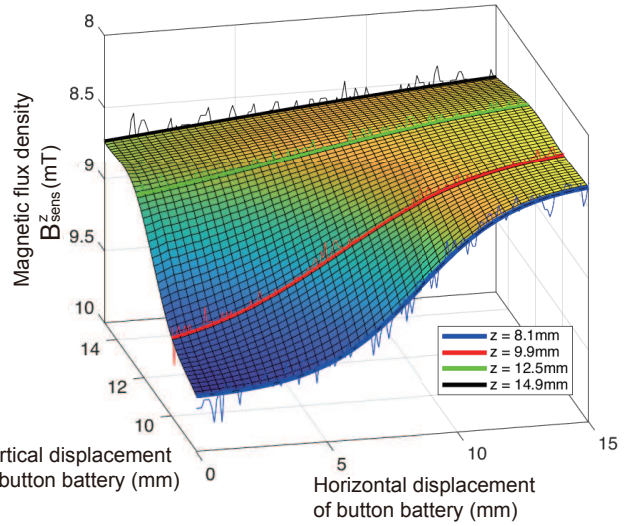

Fig. 4. Magnetic flux density at the sensor position ($\mathbf{B}^z_{sens}$) when changing the location of the button battery horizontally and vertically. The solid curves are sigmoid functions in (5) to approximate the relation between magnetic flux density and the distance between the sensor and the button battery. The sensor noise is also shown in the figure.

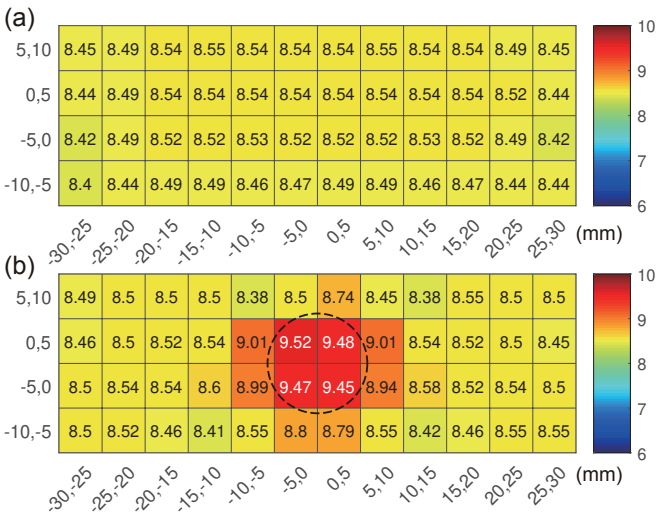

Fig. 5. Sensible location of button battery. (a) Magnetic flux density on the sensing board without button battery. (b) Magnetic flux density on the sensing board with a horizontal sitting button battery at the origin (location indicated with a dotted circle). Each block in the grid represents $5 \times 5\,\mathrm{mm}^2$ area on the sensing board.

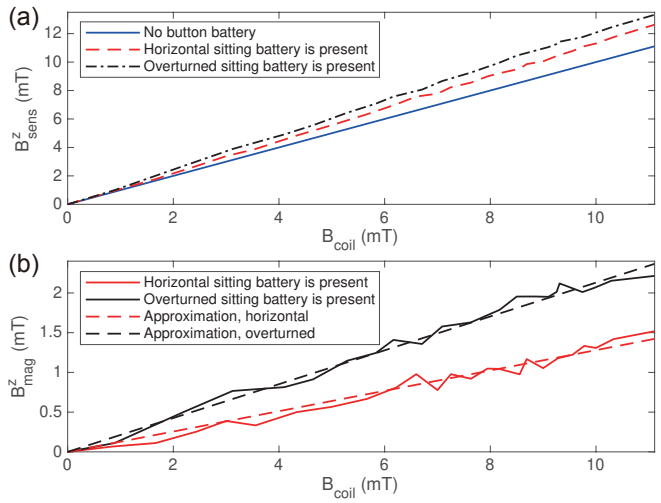

Fig. 6. Difference in $\mathbf{B}^z_{sens}$ with and without the presence of button battery. (a) $\mathbf{B}^z_{sens}$ vs $\mathbf{B}_{coil}$. (b) $\mathbf{B}^z_{mag}$.

in $\mathbf{B}^z_{sens}$ that increases simultaneously with the increase of $\mathbf{B}_{coil}$. The difference $\mathbf{B}^z_{mag}$ can be linearly approximated as shown in Fig. 6 (b) as

$$\mathbf{B}^z_{mag}\ (\text{horizontal}) = 0.128 \cdot \mathbf{B}_{coil}, \tag{16}$$

$$\mathbf{B}^z_{mag}\ (\text{overturned}) = 0.213 \cdot \mathbf{B}_{coil}. \tag{17}$$

(16) and (17) are approximations for horizontal sitting and overturned sitting batteries, respectively. They indicate a progressively stronger magnetization when increasing the strength of the applied field on the battery.

C. Localization test

Experiments were conducted to evaluate the performance of the localization of both the horizontal and overturned sitting batteries. Fig. 7 shows the comparison of the estimated localization results and the real locations of the batteries. It can be seen that the detection region covers all the triangles. We can conclude that in the detection region, it is possible to detect the button battery within an error of less than the size of the button battery. The error of detection is shown in Table II. It can be seen that the accuracy of detecting overturned sitting batteries is higher than detecting horizontal sitting batteries.

TABLE II
DETECTION ERROR

Trials = 20	Avg. ± Std. (mm)	Min (mm)	Max (mm)
Horizontal sitting	3.0931 ± 1.2312	0.3538	5.3069
Overturned sitting	1.3940 ± 1.1231	0.2377	3.4850

D. Automatic dislocation of button battery

The experiment Fig. 8 shows the entire demonstration of automatic dislocation of an LR44 button battery. The button battery was placed in a 2-D phantom stomach of a 3-year-old toddler, that was made using rapid prototyping with polylactic acid, has a maximum length 12.5 cm and a maximum width 11.5 cm. The phantom stomach was filled with water at 3 mm depth to simulate the moisture and damping environment.

With the vertical magnetic field produced by the magnetization coil, the program averaged the sensing data for 30 samples, filtered them, and ran the detection algorithm. Among the measured 20 trials, the average time taken for the battery detection was 2.2 s. Then the algorithm searched for the location of the magnet containing capsule and autonomously navigate the capsule to the button battery (using spinning locomotion). After the capsule attached itself to

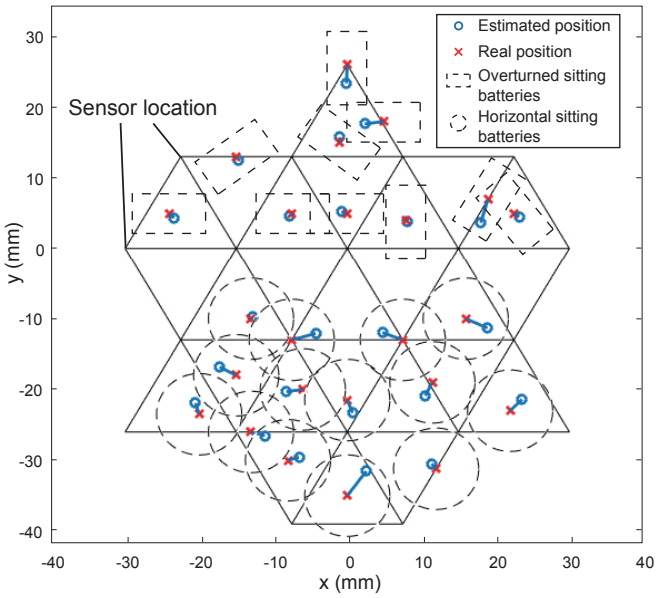

Fig. 7. Evaluation of the button battery localization performance. Red cross: real position of button battery; blue circle: estimated position; black dotted circle and rectangle: button battery size.

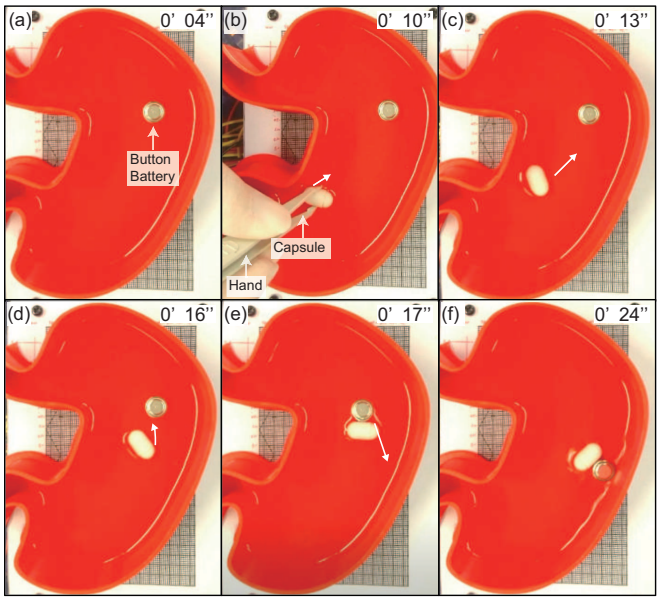

Fig. 8. Automatic dislocation of button battery. (a) Placement of an LR44 button battery in our simulated environment. (b) After localization of the button battery, a capsule robot was placed in the phantom stomach. (c)(d) Magnetically navigated the capsule to the battery position. (e) The capsule attracted to the battery when it was close to the battery. (f) The algorithm detected the attraction and dislocated the battery.

the battery, the algorithm controlled the locomotion of the capsule and dislocated the battery. The size of capsule used in the demonstration, ~ 00 size, was chosen for a demonstration purpose but it is large for a toddler to swallow. The size will be scaled down to the level that still accommodates the magnet and maximize the torque to displace a battery.

IV. Discussions

A. Sensing range of Hall-effect sensor

We estimate that the thickness of the tissue around the torso of a typical 3-year-old boy is $\sim$ 14 cm; therefore, the maximum distance between the stomach wall and the nearest skin surface of a toddler could be 7 cm or farther and even more for an adult. This value is bigger than the range demonstrated in this study.

Fortunately, there are solutions to extend the detection range. The easiest solution is to increase the strength of the applied magnetic field on the button battery. The maximum magnetic field that the horizontal coil can currently produce, ± 11.11 mT, is capped by the maximum current that the current driver and power sources can handle. In addition to improving these factors, we can embed an iron core to the magnetization coil, or utilize the four navigation coils to produce a superposed vertical magnetic field. Another solution is to increase the density of the sensor array to reduce the area of each trilateration triangle, such that the signal strength received by each sensor is enhanced, leading to a more flexible choice of distance required from the sensor to the stomach.

B. Detection of different button batteries

We tested and determined measurements for different types of button batteries and choose the largest and smallest batteries in the experiments for discussion.

1) Cr2032 (20 mm diameter, 3.2 mm height): Cr2032 is a larger battery than LR44 and is also a commonly used button battery. The results of the experiment with this battery showed reliable detection when the battery was overturned sitting. However, it encountered difficulty when detecting the horizontal sitting battery. Only by decreasing the vertical distance between the sensor and the battery (less than 10 mm) could the sensors detect the location.

2) SR66 (6.8 mm diameter, 2.6 mm height): SR66 is a smaller battery than LR44 and is commonly used in many wrist watches. In the experiment, the system failed to detect the location of the battery irrespective to its orientation because of the weak magnetization of the battery under a magnetic field. This is mainly due to the lack of the strength of the magnetic field, which was not strong enough to magnetize the battery. The problem can be solved by increasing the magnetic field, increasing the density of the sensor array, or replacing the Hall-effect sensors to detect a smaller magnetic field.

3) Other ferromagnetic object detection: We conducted similar experiments that localized different types of ferromagnetic objects made of 430 stainless steel. With the current experimental setup, it was possible to detect M4, M5, M6, and M7 screws (overturned sitting), M4 nuts (overturned sitting), and M5, M6, and M7 nuts (both horizontal and overturned sitting).

V. Conclusion

In this study, we proposed a low cost localization method for detecting an ingested button battery using an electromagnetic coil and a Hall-effect sensor array. A button battery was magnetized by applying a magnetic field. Then, by remotely detecting the magnetization with Hall-effect sensors and analyzing the intensity, we were able to localize the position of the button battery. The developed system can then autonomously navigate a magnetic capsule to the location where the battery resides, connect to it, and dislocate it.

The proposed method is applicable for a certain range of ferromagnetic materials with high susceptibility. Future work includes extending with a longer range, 3-D localization, and treatment of dislocated battery, and practice in an close-to-real environment where peristaltic movement is involved.

Acknowledgment

We thank Daniela Rus and Dana D. Damian for the valuable discussions, Haoming Yang for fabricating the horizontal coil and Mo Wang, Zihao Fang, Igors Dubanevics and Yingchun Cao for reviewing the manuscript.

REFERENCES

[1] [Online]. Available: http://poison.org/battery

[2] D. Yardeni, H. Yardeni, A. G. Coran, and E. S. Golladay, "Severe esophageal damage due to button battery ingestion: can it be prevented?" *Pediatric Surgery International*, vol. 20, no. 7, pp. 496–501, Jul 2004.

[3] J. Hee Lee, J. Hoo Lee, J. Ok Shim, J. Hwa Lee, B.-L. Eun, and K. Hwan Yoo, "Foreign body ingestion in children: Should button batteries in the stomach be urgently removed?" *Pediatric gastroenterology, hepatology & nutrition*, vol. 19, pp. 20–28, Mar 2016.

[4] M. Sitti, H. Ceylan, W. Hu, J. Giltinan, M. Turan, S. Yim, and E. Diller, "Biomedical applications of untethered mobile milli/microrobots," *Proceedings of the IEEE*, vol. 103, no. 2, pp. 205–224, Feb 2015.

[5] B. J. Nelson, I. K. Kaliakatsos, and J. J. Abbott, "Microrobots for minimally invasive medicine," *Annual Review of Biomedical Engineering*, vol. 12, no. 1, pp. 55–85, 2010.

[6] E. Diller, S. Floyd, C. Pawashe, and M. Sitti, "Control of multiple heterogeneous magnetic micro-robots on non-specialized surfaces," in *2011 IEEE International Conference on Robotics and Automation*, May 2011, pp. 115–120.

[7] S. Martel, "Beyond imaging: Macro- and microscale medical robots actuated by clinical mri scanners," *Science Robotics*, vol. 2, no. 3, 2017.

[8] A. Ghosh, C. Yoon, F. Ongaro, S. Scheggi, F. M. Selaru, S. Misra, and D. H. Gracias, "Stimuli-responsive soft untethered grippers for drug delivery and robotic surgery," *Frontiers in Mechanical Engineering*, vol. 3, p. 7, 2017.

[9] A. du Plessis d'Argentré, S. Perry, Y. Iwata, H. Iwasaki, E. Iwase, A. Fabozzo, I. Will, D. Rus, D. D. Damian, and S. Miyashita, "Programmable medicine: Autonomous, ingestible, deployable hydrogel patch and plug for stomach ulcer therapy," in *2018 IEEE International Conference on Robotics and Automation (ICRA)*, May 2018, pp. 1511–1518.

[10] S. Fusco, H.-W. Huang, K. E. Peyer, C. Peters, M. Häberli, A. Ulbers, A. Spyrogianni, E. Pellicer, J. Sort, S. E. Pratsinis, B. J. Nelson, M. S. Sakar, and S. Pané, "Shape-switching microrobots for medical applications: The influence of shape in drug delivery and locomotion," *ACS Applied Materials & Interfaces*, vol. 7, no. 12, pp. 6803–6811, 2015.

[11] P. Glass, E. Cheung, and M. Sitti*, "A legged anchoring mechanism for capsule endoscopes using micropatterned adhesives," *IEEE Transactions on Biomedical Engineering*, vol. 55, no. 12, pp. 2759–2767, Dec 2008.

[12] P. Valdastri, M. Simi, and R. J. Webster, "Advanced technologies for gastrointestinal endoscopy," *Annual Review of Biomedical Engineering*, vol. 14, no. 1, pp. 397–429, 2012.

[13] M. Nokata, S. Kitamura, T. Nakagi, T. Inubushi, and S. Morikawa, "Capsule type medical robot with magnetic drive in abdominal cavity," in *2008 2nd IEEE RAS EMBS International Conference on Biomedical Robotics and Biomechatronics*, Oct 2008, pp. 348–353.

[14] J. L. Toennies, G. Tortora, M. Simi, P. Valdastri, and R. J. Webster, "Swallowable medical devices for diagnosis and surgery: The state of the art," *Proceedings of the Institution of Mechanical Engineers, Part C: Journal of Mechanical Engineering Science*, vol. 224, no. 7, pp. 1397–1414, 2010.

[15] M. Quirini, R. J. Webster, A. Menciassi, and P. Dario., "Design of a pill-sized 12-legged endoscopic capsule robot," in *Proceedings 2007 IEEE International Conference on Robotics and Automation*, Apr 2007, pp. 1856–1862.

[16] K. Kong, S. Yim, S. Choi, and D. Jeon, "A Robotic Biopsy Device for Capsule Endoscopy," *Journal of Medical Devices*, vol. 6, no. 3, Jul 2012.

[17] S. Yim, K. Goyal, and M. Sitti, "Magnetically actuated soft capsule with the multimodal drug release function," *IEEE/ASME Transactions on Mechatronics*, vol. 18, no. 4, pp. 1413–1418, Aug 2013.

[18] D. Son, M. D. Dogan, and M. Sitti, "Magnetically actuated soft capsule endoscope for fine-needle aspiration biopsy," in *2017 IEEE International Conference on Robotics and Automation (ICRA)*, May 2017, pp. 1132–1139.

[19] M. P. Kummer, J. J. Abbott, B. E. Kratochvil, R. Borer, A. Sengul, and B. J. Nelson, "Octomag: An electromagnetic system for 5-DOF wireless micromanipulation," *IEEE Transactions on Robotics*, vol. 26, no. 6, pp. 1006–1017, Dec 2010.

[20] S. Martel, C. C. Tremblay, S. Ngakeng, and G. Langlois, "Controlled manipulation and actuation of micro-objects with magnetotactic bacteria," *Applied Physics Letters*, vol. 89, no. 23, p. 233904, 2006.

[21] D. D. Damian, K. Price, S. Arabagi, I. Berra, Z. Machaidze, S. Manjila, S. Shimada, A. Fabozzo, G. Arnal, D. Van Story, J. D. Goldsmith, A. T. Agoston, C. Kim, R. W. Jennings, P. D. Ngo, M. Manfredi, and P. E. Dupont, "In vivo tissue regeneration with robotic implants," *Science Robotics*, vol. 3, no. 14, 2018.

[22] C. Yu, J. Kim, H. Choi, J. Choi, S. Jeong, K. Cha, J. oh Park, and S. Park, "Novel electromagnetic actuation system for three-dimensional locomotion and drilling of intravascular microrobot," *Sensors and Actuators A: Physical*, vol. 161, no. 1, pp. 297–304, 2010.

[23] S. Miyashita, S. Guitron, M. Ludersdorfer, C. R. Sung, and D. Rus, "An untethered miniature origami robot that self-folds, walks, swims, and degrades," in *2015 IEEE International Conference on Robotics and Automation (ICRA)*, May 2015, pp. 1490–1496.

[24] S. Miyashita, S. Guitron, K. Yoshida, Shuguang Li, D. D. Damian, and D. Rus, "Ingestible, controllable, and degradable origami robot for patching stomach wounds," in *2016 IEEE International Conference on Robotics and Automation (ICRA)*, May 2016, pp. 909–916.

[25] S. Miyashita, S. Guitron, S. Li, and D. Rus, "Robotic metamorphosis by origami exoskeletons," *Science Robotics*, vol. 2, no. 10, 2017.

[26] S. Yim and M. Sitti, "3-D localization method for a magnetically actuated soft capsule endoscope and its applications," *IEEE Transactions on Robotics*, vol. 29, no. 5, pp. 1139–1151, Oct 2013.

[27] D. Son, S. Yim, and M. Sitti, "A 5-D localization method for a magnetically manipulated untethered robot using a 2-D array of hall-effect sensors," *IEEE/ASME Transactions on Mechatronics*, vol. 21, no. 2, pp. 708–716, Apr 2016.

[28] S. Guitron, A. Guha, S. Li, and D. Rus, "Autonomous locomotion of a miniature, untethered origami robot using hall effect sensor-based magnetic localization," in *2017 IEEE International Conference on Robotics and Automation (ICRA)*, May 2017, pp. 4807–4813.

[29] Z. Sun, L. Maréchal, and S. Foong, "Passive magnetic-based localization for precise untethered medical instrument tracking," *Computer Methods and Programs in Biomedicine*, vol. 156, pp. 151–161, 2018.

[30] S. Song, B. Li, W. Qiao, C. Hu, H. Ren, H. Yu, Q. Zhang, M. Q. H. Meng, and G. Xu, "6-D magnetic localization and orientation method for an annular magnet based on a closed-form analytical model," *IEEE Transactions on Magnetics*, vol. 50, no. 9, pp. 1–11, Sep. 2014.

[31] K. Seikel, P. A. Primm, B. J. Elizondo, and K. L. Remley, "Handheld Metal Detector Localization of Ingested Metallic Foreign Bodies: Accurate in Any Hands?" *JAMA Pediatrics*, vol. 153, no. 8, pp. 853–857, Aug 1999.

[32] V. James, H. B. Hamzah, and S. Ganapathy, "Handheld metal detector screening for metallic foreign body ingestion in children," *JoVE (Journal of Visualized Experiments)*, no. 139, p. e58468, 2018.

[33] G. Conners, "Diagnostic uses of metal detectors: A review," *International journal of clinical practice*, vol. 59, pp. 946–9, 09 2005.